Time-localized dark modes generated by zero-wave-number-gain modulational instability

Lei Liu,[1] Wen-Rong Sun,[2,*] Boris A. Malomed,[3,4] and P. G. Kevrekidis[5]

[1]*College of Mathematics and Statistics, Chongqing University, Chongqing 401331, China*
[2]*School of Mathematics and Physics, University of Science and Technology Beijing, Beijing 100083, China*
[3]*Department of Physical Electronics, School of Electrical Engineering, Faculty of Engineering, and Center for Light-Matter Interaction, Tel Aviv University, P.O. Box 39040, Ramat Aviv, Tel Aviv, Israel*
[4]*Instituto de Alta Investigación, Universidad de Tarapacá, Casilla 7D, Arica, Chile*
[5]*Department of Mathematics and Statistics, University of Massachusetts, Amherst, Massachusetts 01003, USA*

(Received 21 June 2023; accepted 22 August 2023; published 7 September 2023)

We report the emergence of a previously unexplored species of solitary waves, viz., *time-localized dark modes* in integrable and nonintegrable variants of the massive Thirring model and in the three-wave resonant-interaction system, which are models broadly used in plasma physics, nonlinear optics, and hydrodynamics. They are also interesting as basic models for the propagation of nonlinear waves in media without intrinsic dispersion. An essential finding is that the condition for the existence of time-localized dark modes in these systems, which develop density dips in the course of their evolution, coincides with the condition for the occurrence of the zero-wave-number-gain (ZWG) modulational instability (MI). Systematic simulations reveal that, whenever the ZWG MI is present, such dark modes are generically excited from a chaotic background as patches embedded in complex patterns.

DOI: 10.1103/PhysRevA.108.033504

I. INTRODUCTION

The modulational instability (MI) of a constant-amplitude continuous-wave (cw) background against long-wavelength perturbations is a fundamental phenomenon in nonlinear physics [1–4]. It triggers complex dynamics in water waves [1,2], plasmas [5–7], electric transmission lines [8,9], nonlinear optics [10–20], matter waves [21–34], and other physical media [35,36]. In particular, MI initiates the spontaneous production of self-sustained states, such as soliton trains, breathers, and rogue waves (RWs) [27,37–50].

Similar to MI, solitons are formed as a result of the interplay between dispersive and nonlinear effects [51]. Universal integrable models, such as the Korteweg–de Vries and nonlinear Schrödinger (NLS) equations and the Manakov system, give rise to the commonly known exact solutions for solitons [52,53]. Solutions for traveling solitons can often be generated by the application of a suitable (Galilean or Lorentz) boost to quiescent ones. However, conservation laws (in particular, the conservation of the total norm) suggest that the NLS or similar integrable equations do not admit the existence of time-localized (pulsed) states [46,47]. It may seem that the existence of RWs contradicts this statement, as apparent localization in time t is their basic feature [54,55]. However, unlike bright solitons, RWs exist on top of a cw background, and at fixed t, RW solutions feature local intensity values below and above the cw level in a mutually compensating way, which makes them compatible with the underlying model conservation laws.

In this work, we use two basic integrable systems, viz., the massive Thirring model (MTM) and three-wave resonant-interaction (3WRI) system, to produce wave forms in the form of dark time-localized modes, which, similar to the spatial structure of dark solitons, feature a time-localized dip in the course of their evolution. An important observation is that the existence condition for such temporarily dark solutions in these systems coincides with the condition of the presence of the zero-wave-number-gain (ZWG) MI, i.e., MI with nonzero gain at the zero wave number of modulational perturbations, defined as in Ref. [56]. Moreover, the same systems admit configurations built as multiple sets of such modes, in compliance with the conservation loss. The present work shows the existence and origin of time-localized dark and antidark modes (the latter meaning states with a temporarily localized bulge on top of the cw background).

The rest of this paper is organized as follows. Exact time-localized solutions of the integrable MTM are produced in Sec. II. An analytical investigation of the MI of the flat cw states, with emphasis on the case of the ZWG MI, is presented in Sec. III. Numerical results, which display the generation of complex patterns that include local patches of time-localized modes by random perturbations initially added to the cw background, are summarized in Sec. IV. The other integrable model, whose exact solutions also demonstrate time-localized modes, viz., the three-wave resonant-interaction system, is briefly considered in Sec. V. The paper is concluded by Sec. VI.

II. TIME-LOCALIZED DARK MODES PRODUCED BY THE MTM

The MTM system, written in laboratory coordinates, applies to the evolution of a self-interacting spinor field in the

*Corresponding author: sunwenrong@ustb.edu.cn

one-dimensional field theory [57,58] and constitutes the integrable model which is most proximal to, but different from, the system governing the propagation of light in fiber Bragg gratings [58–62]. The scaled form of the MTM is

$$i\partial_t u_1 + i\partial_x u_1 + u_2 + |u_2|^2 u_1 = 0, \tag{1a}$$

$$i\partial_t u_2 - i\partial_x u_2 + u_1 + |u_1|^2 u_2 = 0. \tag{1b}$$

Here u_1 and u_2 are slowly varying complex envelopes of counterpropagating electromagnetic waves (in terms of optics), and t and x are the normalized time and spatial coordinate, with the group velocities and nonlinearity coefficient scaled to be, respectively, ± 1 and 1. Note that Eqs. (1) can be written in another well-known form in terms of the light-cone coordinates, $(x \pm t)/\sqrt{2}$ [62–64], and can be transformed into the single sine-Gordon equation, which is integrable too [65].

General N-bright and N-dark soliton solutions of the MTM in the light-cone coordinates can be produced by the Hirota bilinear method [64]. We find that, different from conventional solitons, dark and antidark soliton solutions of Eqs. (1) in laboratory coordinates admit a time-localized shape. Note that the MTM does not admit time-localized bright and dark solitons in light-cone coordinates, and bright solitons of Eqs. (1) cannot be time localized either [64].

Fundamental dark- or antidark-mode solutions of Eqs. (1) are written as [64]

$$u_1 = a_1 e^{i\theta(x,t)} \frac{1 + e^{\xi_1+\xi_1^*+i\phi_1+\kappa_1}}{1 + e^{\xi_1+\xi_1^*+\kappa_1}} = a_1 e^{i\theta(x,t)}\left[1 + e^{i\phi_1} + (e^{i\phi_1} - 1)\tanh\left(\xi_1 + \xi_1^* + \frac{\kappa_1}{2}\right)\right], \tag{2a}$$

$$u_2 = a_2 e^{i\theta(x,t)} \frac{1 + e^{\xi_1+\xi_1^*+i\phi_2+\kappa_1}}{1 + e^{\xi_1+\xi_1^*+\kappa_1^*}} = a_2 e^{i\theta(x,t)}\left[1 + e^{i\phi_2} + (e^{i\phi_2} - 1)\tanh\left(\xi_1 + \xi_1^* + \frac{\kappa_1^*}{2}\right)\right], \tag{2b}$$

where

$$\theta(x,t) = \frac{1}{2}(1 + a_1 a_2)\left[\left(\frac{a_2}{a_1} - \frac{a_1}{a_2}\right)x + \left(\frac{a_2}{a_1} + \frac{a_1}{a_2}\right)t\right], \tag{3}$$

$$e^{\kappa_1} = -\frac{i p_1^*}{p_1 + p_1^*},$$
$$e^{i\phi_1} = -\frac{p_1 - i\beta}{p_1^* + i\beta},$$
$$e^{i\phi_2} = -\frac{p_1 - i\beta(1 + a_1 a_2)}{p_1^* + i\beta(1 + a_1 a_2)},$$
$$\xi_1 = \frac{\chi_1}{2}x + \frac{\chi_2}{2}t + \xi^{(0)},$$

$$\chi_j = \frac{a_2}{\beta a_1} p_1 - (-1)^j \frac{\beta a_1}{a_2}(1 + a_1 a_2) p_1^{-1}, \ j = 1, 2. \tag{4}$$

Here $*$ stands for the complex conjugate, while p_1 and $\xi^{(0)}$ and a_1, a_2, and β are complex and real constants, respectively, which must satisfy the following constraint:

$$|p_1 - i\beta(1 + a_1 a_2)|^2 = \beta^2 a_1 a_2 (1 + a_1 a_2). \tag{5}$$

If we separate the real and imaginary parts of the complex parameter, $p_1 \equiv p_{1R} + i p_{1I}$, the component $u_1(x,t)$ of the solution exhibits a temporary dark-mode shape for $\beta p_{1R} < 0$ and an antidark one in the opposite case, while u_2 represents a dark-mode shape at $\beta(1 + a_1 a_2) p_{1R} < 0$ and an antidark-mode one in the opposite case.

Expression (4) for the fully time-localized dark or antidark solution is

$$\chi_1 + \chi_1^* = \frac{p_1 + p_1^*}{\beta |p_1|^2 a_1 a_2}\left[\beta^2 a_1^2 (1 + a_1 a_2) + a_2^2 |p_1|^2\right] = 0. \tag{6}$$

This condition implies the spatial independence of the modulus of the solutions in Eqs. (2a)–(2b). Combining Eqs. (5) and (6), we then obtain

$$\beta(1 + a_1 a_2)\left[2 p_{1I} a_2^2 + \beta\left(a_1^2 - a_2^2\right)\right] = 0. \tag{7}$$

From Eq. (5), we get $\beta(1 + a_1 a_2) \neq 0$; hence, Eq. (7) yields $2 p_{1I} a_2^2 + \beta(a_1^2 - a_2^2) = 0$, which further results in

$$p_{1I} = -\frac{\beta\left(a_1^2 - a_2^2\right)}{2 a_1^2}, \tag{8a}$$

$$p_{1R} = \pm\frac{|\beta a_1 a_2|}{2 a_2^2}\sqrt{-\left(2 + \frac{a_1^2}{a_2^2} + \frac{a_2^2}{a_1^2} + 4 a_1 a_2\right)}. \tag{8b}$$

Because p_{1R} is a nonzero real constant, parameters a_1 and a_2 need to satisfy the constraint

$$2 + \frac{a_1^2}{a_2^2} + \frac{a_2^2}{a_1^2} + 4 a_1 a_2 < 0. \tag{9}$$

In other words, inequality (9) is the existence condition for the time-localized dark modes, where a_1 and a_2 represent the background amplitudes of the dark-mode components u_1 and u_2, respectively. On the other hand, the stationary dark-mode solution can be obtained by setting χ_2 to be purely imaginary. Figures 1(a)–1(d) display examples of stationary states which feature the spatially localized antidark shape in both components (i.e., it is a two-component spatial antidark soliton) and the antidark temporarily localized shape in component u_1 and the temporal dark shape in u_2. The former solution is displayed for the sake of the comparison of the spatial solitons with the time-localized modes.

III. THE LINEAR-STABILITY ANALYSIS OF cw SOLUTIONS AND THE ZWG MI CONDITION

Equations (1) admit the following cw solutions:

$$u_l = a_l e^{i[\theta(x,t)+\theta_0]}, \qquad l = 1, 2, \tag{10}$$

where $\theta(x,t)$ is defined as per Eq. (3) and θ_0 is a real phase shift. To study the linear stability of the cw, we add small complex perturbations $p_l(x,t)$ to it, setting

$$\widetilde{u}_l^p = [a_l + p_l(x,t)] e^{i[\theta(x,t)+\theta_0]}, \qquad l = 1, 2. \tag{11}$$

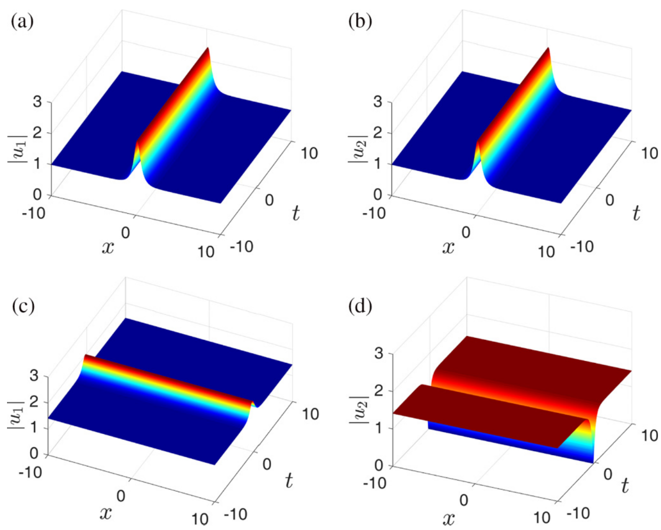

FIG. 1. Solutions produced by Eqs. (1) with parameters $\beta = 1$ and $\xi^{(0)} = 0$. (a) and (b) a stationary two-component spatial antidark soliton with $a_1 = a_2 = 1$ and $p_1 = 1 + i$. (c) and (d) A time-localized half-antidark, half-dark solution with $a_1 = -a_2 = \sqrt{2}$ and $p_1 = 1$

Substituting expressions (11) in Eqs. (1), we derive linearized equations for $p_l(x,t)$,

$$ia_1\partial_t p_1 + ia_1\partial_x p_1 - a_2 p_1 + a_1(1 + a_1a_2)p_2 + a_1^2 a_2 p_2^* = 0, \tag{12a}$$

$$ia_2\partial_t p_2 - ia_2\partial_x p_2 - a_1 p_2 + a_2(1 + a_1a_2)p_1 + a_1 a_2^2 p_1^* = 0. \tag{12b}$$

Assuming, as is customary, $p_l = \eta_{l,1}(t)e^{iQx} + \eta_{l,2}(t)e^{-iQx}$, where Q is a real perturbation wave number and $\eta_{l,1}(t)$ and $\eta_{l,2}(t)$ are complex amplitudes, Eqs. (12) lead to a 4×4 homogeneous linear differential equation in matrix form for $\eta = (\eta_{1,1}, \eta_{1,2}^*, \eta_{2,1}, \eta_{2,2}^*)^T$:

$$\partial_t \eta = i\mathbf{M}\eta, \tag{13}$$

where the matrix elements of $\mathbf{M}$ are $M_{11} = -Q - a_2/a_1$, $M_{22} = -Q + a_2/a_1$, $M_{33} = Q - a_1/a_2$, $M_{44} = Q + a_1/a_2$, $M_{41} = M_{32} = -M_{23} = -M_{14} = a_1a_2$, $M_{13} = M_{31} = -M_{24} = -M_{42} = 1 + a_1a_2$, and $M_{12} = M_{21} = M_{34} = M_{43} = 0$.

The stability of solution (11) is then determined by eigenvalues of matrix $\mathbf{M}$, which are roots of the following characteristic polynomial:

$$\Omega^4 + \lambda_2\Omega^2 + \lambda_1\Omega + \lambda_0 = 0, \tag{14}$$

where we define

$$\lambda_0 = Q^2\left(-\frac{a_1^2}{a_2^2} - \frac{a_2^2}{a_1^2} + 4a_1a_2 + Q^2 + 2\right),$$

$$\lambda_1 = 2Q\left(\frac{a_2^2}{a_1^2} - \frac{a_1^2}{a_2^2}\right),$$

$$\lambda_2 = -2(1 + Q^2) - 4a_1a_2 - \frac{a_1^2}{a_2^2} - \frac{a_2^2}{a_1^2}.$$

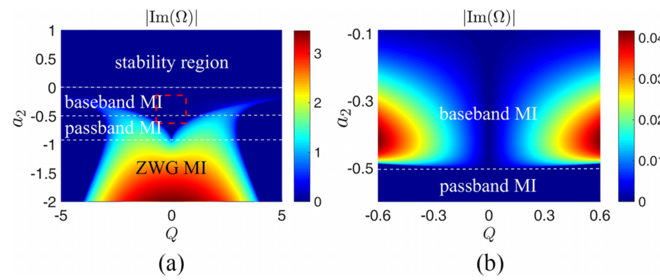

FIG. 2. The color map of the MI gain $|\mathrm{Im}(\Omega)|$ in parameter plane (Q, a_2) of cw solutions (2), as produced by Eqs. (1), with fixed $a_1 = 2$. (b) Zoom of the red box in (a).

Roots of Eq. (14) (Ω_j, $j = 1, 2, 3, 4$) either are real ones or form complex-conjugate pairs. If all the roots are real, there is no MI. If frequencies Ω_j include complex-conjugate pairs, MI is represented by $\mathrm{Im}(\Omega) < 0$. Similar to the setting considered in Ref. [56], MI may be one of three different types:

(i) Baseband MI has $\mathrm{Im}(\Omega) < 0$ at $|Q| > 0$ and $\mathrm{Im}(\Omega) = 0$ at $Q = 0$; that is, the MI band includes arbitrarily small wave numbers Q but *not* $Q = 0$.

(ii) Passband MI has $\mathrm{Im}(\Omega) < 0$ at $|Q| > Q_{\min} > 0$ with a nonzero boundary $Q_{\min}$ of the MI band, which separates it from $Q = 0$.

(iii) ZWG MI has $\mathrm{Im}(\Omega) < 0$ at $|Q| < Q_{\max}$ with $Q_{\max} > 0$; that is, the MI band *includes* the zero wave number, $Q = 0$.

When the MI exists, the boundaries of the ZWG MI region are defined by setting $Q = 0$ in Eqs. (14). Then, two possible nonzero roots of Eqs. (14) are $\pm\sqrt{\Omega_0^2}$, with

$$\Omega_0^2 = 2 + \frac{a_1^2}{a_2^2} + \frac{a_2^2}{a_1^2} + 4a_1a_2. \tag{15}$$

The ZWG MI takes place at $\Omega_0^2 < 0$; otherwise, only baseband or passband MI regions may exist. We stress that this condition *coincides* with the existence condition for the time-localized dark mode, which is given by Eq. (9). This fact strongly indicates that the emergence of time-localized modes is intimately connected to the growth of the modulational perturbation with wave number $Q = 0$.

Figure 2 shows different MI types produced by Eqs. (1) with fixed $a_1 = 2$. In particular, the modulational stability, baseband MI, passband MI, and ZWG MI take place at $a_2 > 0$, $-0.5 \leqslant a_2 < 0$, $-0.897 < a_2 < -0.5$, and $-31.7 < a_2 < -0.897$, respectively (at $a_2 < -31.7$, the passband MI occurs, which is not shown in Fig. 2). On the other hand, at $a_1 = 2$ Eq. (2) produces the time-localized dark modes solely in the last interval, $-31.7 < a_2 < -0.897$.

IV. NUMERICAL SIMULATIONS: EXCITATION OF TIME-LOCALIZED MODES IN THE INTEGRABLE AND NONINTEGRABLE MTM BY CHAOTIC PERTURBATIONS ADDED TO THE BACKGROUND FIELD

The MI evolution is a natural source of solitary waves [10,51,53]. In particular, the MI evolution initiated by random perturbations has drawn interest in optics and hydrodynamics, chiefly in connection to the generation of RWs and breathers [54,66]. To verify the relation between the existence of the

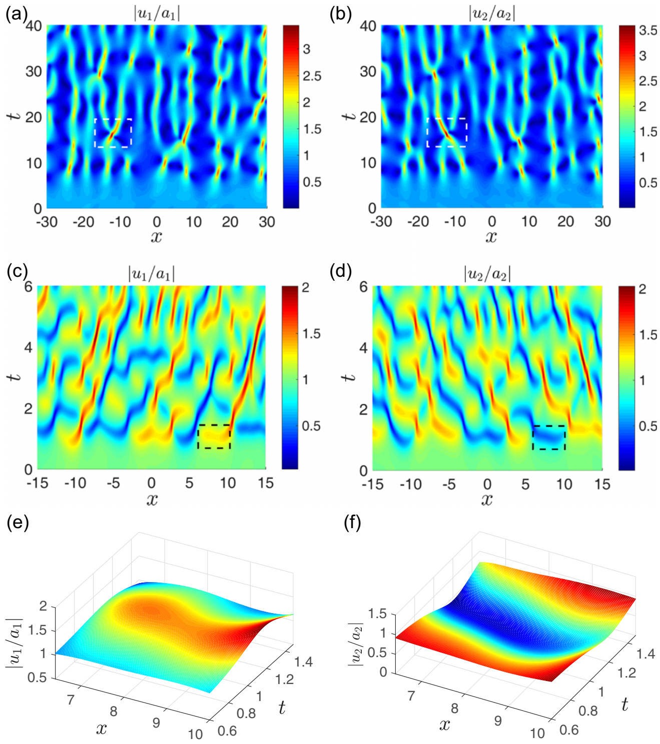

FIG. 3. The numerically simulated excitation of a pattern composed of time-localized dark modes produced by chaotic perturbations with a 5% relative strength initially added to the cw background, where the color map indicates the intensity of $|u_l/a_l|$. The parameters are $a_1 = -a_2 = 0.8$ in (a) and (b), and $a_1 = -a_2 = 2.4$ in (c) and (d). A particular fragment in the form of a dark-antidark localized mode is highlighted by the black box. (e) and (f) display the three-dimensional zoom of this pattern.

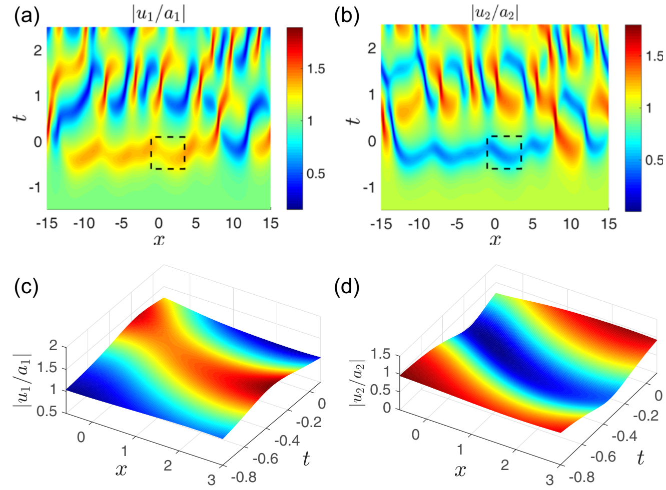

FIG. 4. The simulated evolution of a time-localized mode given by solution (2) with initially added random-noise perturbations at the 2% level, where the color map indicates the intensity of $|u_l/a_l|$. The input is the cw background perturbed by a random noise with 5% strength. The parameters are $\beta = 1$, $\xi^{(0)} = 0$, $a_1 = -a_2 = 2.4$, and $p_1 = \sqrt{119}/3$. The numerical simulation is initiated at $t = -1.5$. A particular fragment of a dark mode is highlighted by a black box. (c) and (d) display the three-dimensional zoom of this pattern.

time-localized dark and antidark modes and ZWG MI, we consider the possibility to excite such modes from a chaotic background field in the presence of the ZWG MI. For this purpose, we simulate the evolution of the cw states taken as the initial condition, perturbed by a random Gaussian noise with a relative strength of 5%.

As demonstrated in Fig. 3, the noisy background features apparent MI-driven chaotic dynamics. For parameters $a_1 = -a_2 = 0.8$ in Figs. 3(a) and 3(b), which satisfy the RW existence condition [56,62,63] but do not satisfy condition (9) for the occurrence of the ZWG MI, isolated peaks with amplitudes $\sim$3 times the background level emerge at random positions. Indeed, these structures in Figs. 3(a) and 3(b) represent RWs.

On the other hand, for parameters $a_1 = -a_2 = 2.4$, which satisfy condition (9), the evolution initiated by the chaotic perturbation produces localized solitonlike structures in Figs. 3(c) and 3(d), while the peak amplitudes are less than 2 times the background level. In particular, a structure which is recognized as a (portion of a) time-localized mode with dark and antidark components, similar to that displayed in Figs. 1(c) and 1(d), is highlighted by a black box in Figs. 3(c) and 3(d). Further, Figs. 3(e) and 3(f) show enlarged three-dimensional plots of this wave pattern.

Similar to RWs, the time-localized dark modes are sensitive to the presence of perturbations because their background is subject to MI. Figure 4 exhibits the evolution of the time-localized mode with initially added 2% random Gaussian-noise perturbations. It is observed that, although the quasisoliton pattern is affected by the background instability, fragments of the time-localized dark state, which are also localized in the x direction, persist as robust elements of the emerging complex pattern, as shown in Figs. 4(c) and 4(d) by the three-dimensional zoom of the fragment highlighted by the black boxes in Figs. 4(a) and 4(b). Note that Figs. 3(e) and 3(f) and 4(c) and 4(d) exhibit similar coupled dark-antidark structures, implying that, in Figs. 3(c) and 3(d), the ZWG MI indeed produces complex patterns incorporating time-localized modes.

It is quite interesting to find time-localized dark (and antidark) modes as solutions of the coupled-mode equations (the nonintegrable version of the MTM) which furnish, as mentioned above, a model for light propagation in periodic or Bragg nonlinear optical media. The respective nonintegrable extensions of Eqs. (1) are

$$i\partial_t u_1 + i\partial_x u_1 + u_2 + (|u_2|^2 + \gamma|u_1|^2)u_1 = 0, \quad (16a)$$

$$i\partial_t u_2 - i\partial_x u_2 + u_1 + (|u_1|^2 + \gamma|u_2|^2)u_2 = 0. \quad (16b)$$

They differ from the integrable MTM by the presence of the self-phase modulation (SPM) with relative strength γ. A straightforward extension of the above analysis produces the following existence condition for the ZWG MI in the present case:

$$2 + \frac{a_1^2}{a_2^2} + \frac{a_2^2}{a_1^2} + 4(1-\gamma)a_1 a_2 < 0 \quad (17)$$

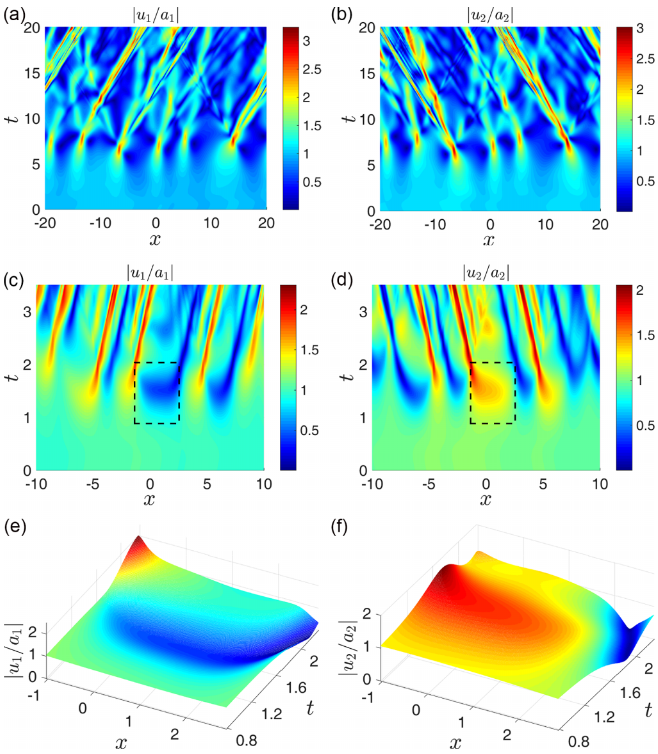

FIG. 5. The excitation of a pattern composed of time-localized dark modes, as produced by simulations of Eq. (16) with $\gamma = 0.5$, where the color map indicates the intensity of $|u_l/a_l|$. The input is the cw background perturbed by a random noise with 5% strength. The parameters are $a_1 = -a_2 = 0.8$ (corresponding to the baseband MI) in (a) and (b) and $a_1 = -a_2 = 2.4$ (the ZWG MI) in (c) and (d). A particular time-localized dark mode is highlighted by the black box. (e) and (f) display the three-dimensional zoom of this state.

[see Eq. (9)]. For example, for the physically relevant case of $\gamma = 0.5$, Fig. 5 displays patterns which are quite similar to those in Fig. 3. This result confirms that the ZWG MI mechanism of the creation of the time-localized modes naturally extends to the physically relevant nonintegrable system and produces an experimentally available setting where such states may be created. It is also relevant to mention bright time-localized modes, which were very recently predicted as solutions of Eqs. (16) [67]. Unlike the present considerations, those bright temporal waves are not related to the cw background and MI conditions.

V. THE THREE-WAVE RESONANT-INTERACTION SYSTEM

To demonstrate that the mechanism elaborated above can be readily implemented in other systems, we consider the system for complex amplitudes $E_n = E_n(x, t)$ $(n = 1, 2, 3)$ of three waves coupled by the quadratic interactions

$$\partial_t E_1 + V_1 \partial_x E_1 = \sigma_1 E_2^* E_3^*, \tag{18a}$$

$$\partial_t E_2 + V_2 \partial_x E_2 = \sigma_2 E_1^* E_3^*, \tag{18b}$$

$$\partial_t E_3 + V_3 \partial_x E_3 = \sigma_3 E_1^* E_2^*. \tag{18c}$$

Here V_n are group velocities of the components, and $\sigma_n = \pm 1$ are signs of the interactions, which correspond to the stimulated-backscattering regime ($\sigma_1 = \sigma_2 = -\sigma_3 = 1$ or $\sigma_1 = -\sigma_2 = -\sigma_3 = 1$), explosive regime ($\sigma_1 = \sigma_2 = \sigma_3 = 1$), or soliton-exchange regime ($\sigma_1 = -\sigma_2 = \sigma_3 = 1$). As a fundamental model, system (18) describes diverse physical contexts in hydrodynamics, optics, and plasmas [68–70]. Without loss of generality, we set $V_1 > V_2 > V_3 \equiv 0$ in the reference frame comoving with wave E_3.

It is well known that system (18) is completely integrable [68,71,72]. The bilinear form [73] of system (18) (the Hirota method) produces the fundamental three-component dark-mode solutions admitted by the integrable system:

$$E_1 = \rho_1 e^{i\phi_1} \frac{1 - \frac{1}{p_1+p_1^*}\frac{p_1-i}{p_1^*+i} e^{\eta_1+\eta_1^*}}{1 + \frac{1}{p_1+p_1^*} e^{\eta_1+\eta_1^*}}, \tag{19a}$$

$$E_2 = \rho_2 e^{i\phi_2} \frac{1 - \frac{1}{p_1+p_1^*}\frac{p_1^*}{p_1} e^{\eta_1+\eta_1^*}}{1 + \frac{1}{p_1+p_1^*} e^{\eta_1+\eta_1^*}}, \tag{19b}$$

$$E_3 = i\rho_3 e^{-i(\phi_1+\phi_2)} \frac{1 + \frac{1}{p_1+p_1^*}\frac{p_1^*+i}{p_1-i}\frac{p_1}{p_1^*} e^{\eta_1+\eta_1^*}}{1 + \frac{1}{p_1+p_1^*} e^{\eta_1+\eta_1^*}}, \tag{19c}$$

where

$$\phi_l = c_l x + d_l t, \ (l = 1, 2), d_1 = d_2 = \frac{\gamma_3}{2},$$

$$c_{1,2} = -\frac{2\gamma_{1,2} + \gamma_3}{2V_{1,2}}, \quad \eta_1 = \frac{1}{p_1} r + \frac{1}{p_1 - i} s + \eta_1^{(0)},$$

$$r = \frac{\gamma_1}{V_1 - V_2}(x - V_2 t), \quad s = \frac{\gamma_2}{V_2 - V_1}(x - V_1 t).$$

Here ρ_n are nonzero real constants representing the background amplitudes of the dark-soliton components E_n; p_1 and $\eta_1^{(0)}$ are complex constants,

$$\gamma_1 = \sigma_1 \frac{\rho_2 \rho_3}{\rho_1}, \gamma_2 = \sigma_2 \frac{\rho_1 \rho_3}{\rho_2}, \gamma_3 = \sigma_3 \frac{\rho_1 \rho_2}{\rho_3}, \tag{20}$$

and these parameters satisfy the following constraint:

$$\frac{\gamma_1 V_2}{|p_1|^2 \gamma_3 (V_2 - V_1)} - \frac{\gamma_2 V_1}{|p_1 - i|^2 \gamma_3 (V_2 - V_1)} = 1. \tag{21}$$

To cast the exact solution of system (18) in the form of a time-localized mode, we set

$$\mathrm{Re}\left\{ \frac{1}{p_1}\frac{\gamma_1}{V_1 - V_2} + \frac{1}{p_1 - i}\frac{\gamma_2}{V_2 - V_1} \right\} = 0, \tag{22}$$

which yields

$$|p_1 - i|^2 \gamma_1 - |p_1|^2 \gamma_2 = 0. \tag{23}$$

Once again this condition ensures the spatial independence of the solution modulus on the spatial variable x. Combining Eqs. (21) and (23) and setting $p_1 = p_{1R} + i p_{1I}$, we obtain

$$p_{1R} = \pm \frac{\sqrt{4\gamma_1\gamma_2 - (\gamma_1 + \gamma_2 - \gamma_3)^2}}{2\gamma_3}, \ p_{1I} = \frac{\gamma_1 - \gamma_2 + \gamma_3}{2\gamma_3}. \tag{24}$$

As p_{1R} takes nonzero real values, parameters γ_1, γ_2, and γ_3 need to satisfy the constraint

$$(\gamma_1 + \gamma_2 - \gamma_3)^2 - 4\gamma_1\gamma_2 < 0. \tag{25}$$

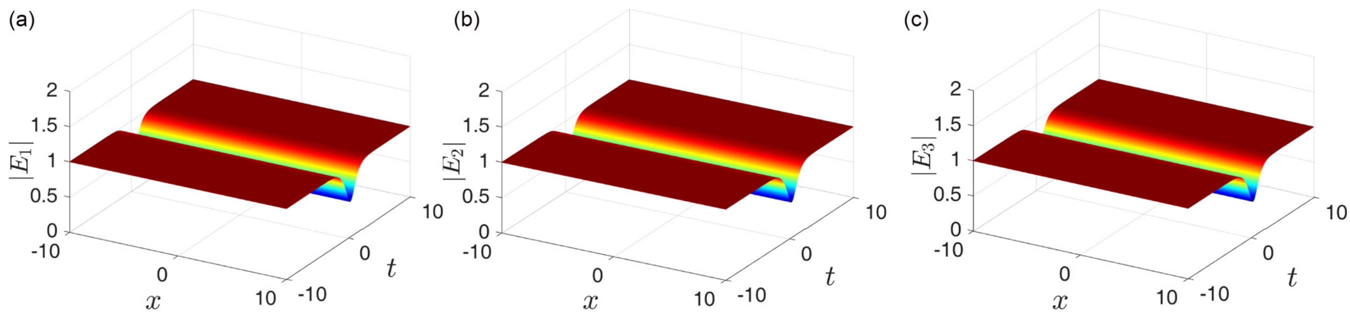

FIG. 6. An example of a time-localized dark mode produced by system (18) with parameters $\sigma_1 = \sigma_2 = \sigma_3 = 1$, $V_1 = 2$, $V_2 = 1$, $a_1 = a_2 = a_3 = 1$, $\eta_1^{(0)} = 0$, and $p_1 = \frac{1}{2}(\sqrt{3} + i)$.

Thus, Eq. (25) is the existence condition for the time-localized dark modes as solutions of system (18).

Following Ref. [56], the condition of the ZWG MI for system (18) is found as $(\gamma_1 + \gamma_2 - \gamma_3)^2 - 4\gamma_1\gamma_2 < 0$. Therefore, we conclude that the condition of the occurrence of the ZWG MI is, once again, tantamount to the existence condition for the time-localized dark mode. This solution is shown in Fig. 6.

VI. CONCLUSION

The present work revealed the existence and origin of a species of dark and antidark quasisoliton states in the form of time-localized modes. Exact solutions of this type were produced in two distinct integrable systems, viz., the MTM and 3WRI system. They provide fundamental models for the propagation of nonlinear waves in media without intrinsic dispersion, which have straightforward realizations in plasmas, nonlinear optics, and hydrodynamics. In the MTM, the time-localized modes feature a dark structure in one component and an antidark one in the other, a feature that is explained on the basis of the associated norm-conservation law. An important conclusion of the analysis is that the existence condition for the time-localized modes in both models is tantamount to the condition providing the occurrence of the ZWG MI. This is a natural conclusion, as it is the MI gain at the zero modulation wave number, $Q = 0$, that generates, respectively, the dip and spike in the dark and antidark components of the mode. Our simulations demonstrated that random perturbations, added to the cw background, give rise to complex patterns composed of robust fragments in the form of the time-localized modes. Furthermore, we demonstrated that the ZWG-MI-based mechanism creates the similar time-localized patterns (or fractions thereof) in the nonintegrable generalization of the MTM, which includes the SPM terms, governing light propagation in Bragg gratings. Hence, it should be possible to create the predicted time-localized modes experimentally in nonlinear optics. To illustrate the generality of the predictions, an additional system featuring such time-localized modes was also presented in the form of the three-wave resonant-interaction system.

As a development of the present analysis, it will be relevant to study in detail multisoliton complexes of the time-localized type, as well as their interactions with the usual spatial solitons or rogue waves. The present study also suggests that the search for time-localized modes in other ZWG-bearing systems is a promising direction for future work.

ACKNOWLEDGMENTS

This work has been supported by the National Natural Science Foundation of China under Grant No. 12205029 and by the Fundamental Research Funds of the Central Universities (Grant No. 230201606500048). The work of B.A.M. is supported, in part, by the Israel Science Foundation (Grant No. 1695/22). The work of P.G.K. is supported by the U.S. National Science Foundation under Grants No. PHY-2110030 and No. DMS-2204702.

[1] T. B. Benjamin and J. E. Feir, The disintegration of wave trains on deep water: Part 1. Theory, J. Fluid Mech. **27**, 417 (1967).
[2] T. B. Benjamin, Instability of periodic wavetrains in nonlinear dispersive systems, Proc. R. Soc. London, Ser. A **299**, 59 (1967).
[3] V. E. Zakharov and L. A. Ostrovsky, Modulation instability: The beginning, Phys. D (Amsterdam, Neth.) **238**, 540 (2009).
[4] G. Vanderhaegen, C. Naveau, P. Szriftgiser, A. Kudlinski, M. Conforti, A. Mussot, M. Onorato, S. Trillo, A. Chabchoub, and N. Akhmediev, Extraordinary modulation instability in optics and hydrodynamics, Proc. Natl. Acad. Sci. USA **118**, e2019348118 (2021).
[5] T. Taniuti and H. Washimi, Self-Trapping and Instability of Hydromagnetic Waves along the Magnetic Field in a Cold Plasma, Phys. Rev. Lett. **21**, 209 (1968).
[6] S. Watanabe, Self-modulation of a nonlinear ion wave packet, J. Plasma Phys. **17**, 487 (1977).
[7] H. Bailung and Y. Nakamura, Observation of modulational instability in a multi-component plasma with negative ions, J. Plasma Phys. **50**, 231 (1993).
[8] P. Marquie, J. M. Bilbault, and M. Remoissenet, Generation of envelope and hole solitons in an experimental transmission line, Phys. Rev. E **49**, 828 (1994).

[9] E. Kengne, W.-M. Liu, L. Q. English, and B. A. Malomed, Ginzburg-Landau models of nonlinear electric transmission networks, Phys. Rep. **982**, 1 (2022).

[10] A. Hasegawa, Generation of a train of soliton pulses by induced modulational instability in optical fibers, Opt. Lett. **9**, 288 (1984).

[11] K. Tai, A. Hasegawa, and A. Tomita, Observation of Modulational Instability in Optical Fibers, Phys. Rev. Lett. **56**, 135 (1986).

[12] S. Trillo and S. Wabnitz, Dynamics of the nonlinear modulational instability in optical fibers, Opt. Lett. **16**, 986 (1991).

[13] M. Yu, C. J. McKinstrie, and G. P. Agrawal, Modulational instability in dispersion-flattened fibers, Phys. Rev. E **52**, 1072 (1995).

[14] F. K. Abdullaev, S. A. Darmanyan, A. Kobyakov, and F. Lederer, Modulational instability in optical fibers with variable dispersion, Phys. Lett. A **220**, 213 (1996).

[15] S. Coen and M. Haelterman, Modulational Instability Induced by Cavity Boundary Conditions in a Normally Dispersive Optical Fiber, Phys. Rev. Lett. **79**, 4139 (1997).

[16] W. Krolikowski, O. Bang, N. I. Nikolov, D. Neshev, J. Wyller, J. J. Rasmussen, and D. Edmundson, Modulational instability, solitons and beam propagation in spatially nonlocal nonlinear media, J. Opt. Soc. Am. B **6**, S288 (2004).

[17] M. Peccianti, C. Conti, G. Assanto, A. De Luca, and C. Umeton, Routing of anisotropic spatial solitons and modulational instability in liquid crystals, Nature (London) **432**, 733 (2004).

[18] J. Meier, G. I. Stegeman, D. N. Christodoulides, Y. Silberberg, R. Morandotti, H. Yang, G. Salamo, M. Sorel, and J. S. Aitchison, Experimental Observation of Discrete Modulational Instability, Phys. Rev. Lett. **92**, 163902 (2004).

[19] M. Centurion, M. A. Porter, Y. Pu, P. G. Kevrekidis, D. J. Frantzeskakis, and D. Psaltis, Modulational Instability in a Layered Kerr Medium: Theory and Experiment, Phys. Rev. Lett. **97**, 234101 (2006).

[20] Y. V. Kartashov and D. V. Skryabin, Modulational instability and solitary waves in polariton topological insulators, Optica **3**, 1228 (2016).

[21] V. V. Konotop and M. Salerno, Modulational instability in Bose-Einstein condensates in optical lattices, Phys. Rev. A **65**, 021602(R) (2002).

[22] L. Salasnich, A. Parola, and L. Reatto, Modulational Instability and Complex Dynamics of Confined Matter-Wave Solitons, Phys. Rev. Lett. **91**, 080405 (2003).

[23] G. Theocharis, Z. Rapti, P. G. Kevrekidis, D. J. Frantzeskakis, and V. V. Konotop, Modulational instability of Gross-Pitaevskii-type equations in $1+1$ dimensions, Phys. Rev. A **67**, 063610 (2003).

[24] L. D. Carr and J. Brand, Spontaneous Soliton Formation and Modulational Instability in Bose-Einstein Condensates, Phys. Rev. Lett. **92**, 040401 (2004).

[25] P. G. Kevrekidis and D. J. Frantzeskakis, Pattern forming dynamical instabilities of Bose-Einstein condensates, Mod. Phys. Lett. B **18**, 173 (2004).

[26] S. Rojas-Rojas, R. A. Vicencio, M. I. Molina, and F. Kh. Abdullaev, Nonlinear localized modes in dipolar Bose-Einstein condensates in optical lattices, Phys. Rev. A **84**, 033621 (2011).

[27] J. H. V. Nguyen, D. Luo, and R. G. Hulet, Formation of matter-wave soliton trains by modulational instability, Science **356**, 422 (2017).

[28] P. J. Everitt, M. A. Sooriyabandara, M. Guasoni, P. B. Wigley, C. H. Wei, G. D. McDonald, K. S. Hardman, P. Manju, J. D. Close, C. C. N. Kuhn, S. S. Szigeti, Y. S. Kivshar, and N. P. Robins, Observation of a modulational instability in Bose-Einstein condensates, Phys. Rev. A **96**, 041601(R) (2017).

[29] T. Mithun, A. Maluckov, K. Kasamatsu, B. Malomed, and A. Khare, Inter-component asymmetry and formation of quantum droplets in quasi-one-dimensional binary Bose gases, Symmetry **12**, 174 (2020).

[30] I. A. Bhat, T. Mithun, B. A. Malomed, and K. Porsezian, Modulational instability in binary spin-orbit-coupled Bose-Einstein condensates, Phys. Rev. A **92**, 063606 (2015).

[31] T. Mithun and K. Kasamatsu, Modulation instability associated nonlinear dynamics of spin–orbit coupled Bose–Einstein condensates, J. Phys. B **52**, 045301 (2019).

[32] C. B. Tabi, S. Veni, and T. C. Kofané, Generation of matter waves in Bose-Bose mixtures with helicoidal spin-orbit coupling, Phys. Rev. A **104**, 033325 (2021).

[33] A. Cidrim, L. Salasnich, and T. Macrí, Soliton trains after interaction quenches in Bose mixtures, New J. Phys. **23**, 023022 (2021).

[34] I. A. Bhat, S. Sivaprakasam, and B. A. Malomed, Modulational instability and soliton generation in chiral Bose-Einstein condensates with zero-energy nonlinearity, Phys. Rev. E **103**, 032206 (2021).

[35] A. M. Kamchatnov, New approach to periodic solutions of integrable equations and nonlinear theory of modulational instability, Phys. Rep. **286**, 199 (1997).

[36] N. Boechler, G. Theocharis, S. Job, P. G. Kevrekidis, Mason A. Porter, and C. Daraio, Discrete Breathers in One-Dimensional Diatomic Granular Crystals, Phys. Rev. Lett. **104**, 244302 (2010).

[37] M. J. Lighthill, Contribution to the theory of waves in non-linear dispersive systems, IMA J. Appl. Math. **1**, 269 (1965).

[38] G. B. Whitham, A general approach to linear and nonlinear dispersive waves using a Lagrangian, J. Fluid Mech. **22**, 273 (1965).

[39] V. I. Bespalov and V. I. Talanov, Filamentary structure of light beams in nonlinear liquids, JETP Lett. **3**, 307 (1966).

[40] V. E. Zakharov, Stability of periodic waves of finite amplitude on a surface of deep fluid, J. Appl. Mech. Tech. Phys. **9**, 190 (1968).

[41] K. B. Dysthe and K. Trulsen, Note on breather type solutions of the NLS as models for freak-waves, Phys. Scr. **T82**, 48 (1999).

[42] A. I. Dyachenko and V. E. Zakharov, Modulation instability of Stokes wave, freak wave, JETP Lett. **81**, 255 (2005).

[43] J. M. Dudley, F. Dias, M. Erkintalo, and G. Genty, Instabilities, breathers and rogue waves in optics, Nat. Photonics **8**, 755 (2014).

[44] M. Onorato, S. Residori, U. Bortolozzo, A. Montina, and F. T. Arecchi, Rogue waves and their generating mechanisms in different physical contexts, Phys. Rep. **528**, 47 (2013).

[45] F. Baronio, M. Conforti, A. Degasperis, S. Lombardo, M. Onorato, and S. Wabnitz, Vector Rogue Waves and Baseband Modulation Instability in the Defocusing Regime, Phys. Rev. Lett. **113**, 034101 (2014).

[46] W. R. Sun, L. Liu, and P. G. Kevrekidis, Rogue waves of ultra-high peak amplitude: A mechanism for reaching up to

a thousand times the background level, Proc. R. Soc. A. **477**, 20200842 (2021).

[47] S. Chen, C. Pan, Ph. Grelu, F. Baronio, and N. Akhmediev, Fundamental Peregrine Solitons of Ultrastrong Amplitude Enhancement through Self-Steepening in Vector Nonlinear Systems, Phys. Rev. Lett. **124**, 113901 (2020).

[48] C. Liu, Y. H. Wu, S. C. Chen, X. Yao, and N. Akhmediev, Exact Analytic Spectra of Asymmetric Modulation Instability in Systems with Self-Steepening Effect, Phys. Rev. Lett. **127**, 094102 (2021).

[49] L. Ling and L. C. Zhao, Rogue wave patterns and modulational instability in nonlinear Schrödinger hierarchy, in *Nonlinear Systems and their Remarkable Mathematical Structures*, Contributions from China Vol. 3 (Chapman and Hall/CRC, 2021), p. 325.

[50] F. Baronio, S. Chen, P. Grelu, S. Wabnitz, and M. Conforti, Baseband modulation instability as the origin of rogue waves, Phys. Rev. A **91**, 033804 (2015).

[51] Y. S. Kivshar and G. P. Agrawal, *Optical Solitons: From Fibers to Photonic Crystals* (Academic, San Diego, 2003).

[52] M. J. Ablowitz and H. Segur, *Solitons and the Inverse Scattering Transform* (SIAM, Philadelphia, PA, 1981).

[53] M. Ablowitz, *Nonlinear Dispersive Waves, Asymptotic Analysis and Solitons* (Cambridge University Press, Cambridge, 2011).

[54] N. Akhmediev, A. Ankiewicz, and J. M. Soto-Crespo, Rogue waves and rational solutions of the nonlinear Schrödinger equation, Phys. Rev. E **80**, 026601 (2009).

[55] N. Akhmediev *et al.*, Roadmap on optical rogue waves and extreme events, J. Opt. **18**, 063001 (2016).

[56] L. Liu, W.-R. Sun, and B. A. Malomed, Formation of Rogue Waves and Modulational Instability with Zero-Wavenumber Gain in Multicomponent Systems with Coherent Coupling, Phys. Rev. Lett. **131**, 093801 (2023)

[57] W. Thirring, A soluble relativistic field theory, Ann. Phys. (NY) **3**, 91 (1958).

[58] A. Degasperis, Darboux polynomial matrices: The classical massive Thirring model as a study case, J. Phys. A **48**, 235204 (2015).

[59] D. N. Christodoulides and R. I. Joseph, Slow Bragg Solitons in Nonlinear Periodic Structures, Phys. Rev. Lett. **62**, 1746 (1989).

[60] A. B. Aceves and S. Wabnitz, Self-induced transparency solitons in nonlinear refractive periodic media, Phys. Lett. A **141**, 37 (1989).

[61] A. M. Kamchatnov, H. Steudel, and A. A. Zabolotskii, The Thirring model as an approximation to the theory of two-photon propagation, J. Phys. A **30**, 7485 (1997).

[62] A. Degasperis, S. Wabnitz, and A. B. Aceves, Bragg grating rogue wave, Phys. Lett. A **379**, 1067 (2015).

[63] J. Chen, B. Yang, and B.-F. Feng, Rogue waves in the massive Thirring model, Stud. Appl. Math. (2023), doi:10.1111/sapm.12619.

[64] J. Chen and B. F. Feng, Tau-function formulation for bright, dark soliton and breather solutions to the massive Thirring model, Stud. Appl. Math. **150**, 35 (2023).

[65] S. Coleman, Quantum sine-Gordon equation as the massive Thirring model, Phys. Rev. D **11**, 2088 (1975).

[66] J. M. Soto-Crespo, N. Devine, and N. Akhmediev, Integrable Turbulence and Rogue Waves: Breathers or Solitons? Phys. Rev. Lett. **116**, 103901 (2016).

[67] Y. Pan, M.-I. Cohen, and M. Segev, Superluminal k-Gap Solitons in Nonlinear Photonic Time Crystals, Phys. Rev. Lett. **130**, 233801 (2023).

[68] A. Bers, D. J. Kaup, and A. H. Reiman, Nonlinear Interactions of Three Wave Packets in a Homogeneous Medium, Phys. Rev. Lett. **37**, 182 (1976).

[69] D. J. Kaup, A. Reiman, and A. Bers, Space-time evolution of nonlinear three-wave interactions. I. Interaction in a homogeneous medium, Rev. Mod. Phys. **51**, 275 (1979).

[70] F. Baronio, M. Conforti, A. Degasperis, and S. Lombardo, Rogue Waves Emerging from the Resonant Interaction of Three Waves, Phys. Rev. Lett. **111**, 114101 (2013).

[71] M. Conforti, F. Baronio, and A. Degasperis, Modulational instability of dark solitons in three wave resonant interaction, Phys. D (Amsterdam, Neth.) **240**, 1362 (2011).

[72] G. Zhang, Z. Yan, and X. Y. Wen, Three-wave resonant interactions: Multi-dark-dark-dark solitons, breathers, rogue waves, and their interactions and dynamics, Phys. D (Amsterdam, Neth.) **366**, 27 (2018).

[73] B. Yang and J. Yang, General rogue waves in the three-wave resonant interaction systems, IMA J. Appl. Math. **86**, 378 (2021).